



Persistent Deformation in a Post-Collisional Stable Continental Region: Insights from 20 Years of cGPS in Romania

Alexandra Muntean^{1*}, Laura Petrescu^{1,2}, Boudewijn Ambrosius³, Felix Borleanu¹, Eduard Ilie Nastase¹, Ioan Munteanu^{4,5}

1. National Institute for Earth Physics, Magurele, 077125, Romania
2. Faculty of Physics, University of Bucharest, Magurele, 077125, Romania
3. Faculty of Aerospace Engineering, Delft University of Technology, Delft, 2629HS, The Netherlands
4. Faculty of Geology and Geophysics, University of Bucharest, Bucharest, 010041, Romania
5. Romanian Academy Institute for Geodynamics “Sabba Stefanescu”, Bucharest, 020032, Romania

Correspondence to: Alexandra Muntean (muntean@infp.ro), Laura Petrescu (laura.petrescu@infp.ro), Boudewijn Ambrosius (bacambrosius@gmail.com).

Abstract

The Carpathian Region, located at the edge of the East European Platform, presents a unique tectonic setting where major deformation associated with subduction and collision appears to have ceased around 8 million years ago. Yet vertical movements and present day seismicity continued afterwards, suggesting ongoing crustal deformation and challenging our understanding of intraplate earthquakes and the processes driving these phenomena in an area considered as a stable continental interior. In this study, we analyse over two decades of continuous GPS (cGPS) data from 143 permanent stations to estimate both horizontal and vertical crustal motions, constructing the most accurate model of crustal deformation in the region to date. The estimated velocity field indicates a southward drift of the South Carpathians and Moesia relative to Eurasia, with velocities ranging from 0.5 to 2 mm/yr. We detect a more complex pattern of vertical uplift and subsidence in the foredeep, challenging a previously held view that this region is solely subsiding. This pattern may reflect localized uplift in response to processes such as the Vrancea slab break-off beneath the South-East Carpathians. Crustal scale active faults accommodate the observed differential motion, fragmenting the foreland. Furthermore, using a regularized horizontal velocity vector field, we estimate strain rate variations, maximum shear strain, and dilatation patterns across Romania, which closely align with observed crustal earthquake mechanisms. This agreement validates our results and indicates a significant influence of surface plate kinematics on the observed seismicity, in addition to the deep Vrancea slab dynamics. Our findings provide fundamental insights into the causes of crustal deformation at the transition between active collision zones and stable continental platforms, enhancing our understanding of intraplate seismicity in regions traditionally considered tectonically stable.

Keywords: deformation, GPS, crustal motion, geology, tectonics

1. Introduction

A key tectonic question lies in understanding the nature of active deformation and frequent seismicity in regions situated at the transition between active subduction/collision systems and more stable continental interiors. The Carpathian Region in Romania marks such a transition between the active Africa-Eurasia subduction system to



the south and the stable continental core of Eurasia: the East European Platform (Fig. 1). Although this area is not considered a traditionally active plate boundary, with most geological evidence suggesting that major deformation associated with the collision ceased around 8 million years ago (Maţenco and Bertotti, 2000), it continues to experience frequent crustal and subcrustal seismicity. Active deformation and seismicity are observed along major faults and geological contacts (e.g. swarms near Tg. Jiu and Galaţi, Craiu et al., 2023, Borleanu et al., 2024). Notably, the Vrancea slab, a relic lithospheric plate sinking, retreating and stretching beneath the East Carpathians Bend Zone, may still be coupled with the overlying crust, as suggested by the thermochronological studies, which showed a significant amount of uplift, post 8 Ma, especially along the Western flank of Focsani Basin (Necea et al., 2021, Fig. S1 in the Supplementary Material). This coupling could be driving long-term surface deformation (Ismail-Zadeh, 2012; Petrescu et al., 2021), contributing to ongoing seismicity (Radulian et al., 2019, 2023) and exhibiting the largest present-day strain concentration in continental Europe (Wenzel et al., 1999).

Measuring crustal motion is crucial for understanding ongoing deformation processes and seismic hazards in such a tectonically complex region. In this study, we estimate both horizontal and vertical motions using Global Positioning System (GPS) data from permanent stations that operated in Romania in the past 20 years. These measurements provide key information about how the region is deforming and how this relates to the observed seismicity. The data also shed light on the connection between surface deformation and subsurface dynamics, including the potential role of the sinking slab in driving seismic activity. Furthermore, the GPS data allows us to assess whether deformation is concentrated along major fault zones or more broadly distributed across the crust, offering a clearer picture of how past tectonic events continue to shape the region's seismic behavior.

The first vertical velocity maps of Romania, based on repeated leveling data from first- and second-order national network lines, were published by Cornea et al. (1977, 1978, 1979). Following the major earthquake of March 4, 1977 (M7.2), high-accuracy leveling measurements allowed for the development of a more refined vertical velocity map (Popescu and Dragoescu, 1987). Subsequent research extended these efforts to the broader Carpatho-Balkan region (Joo et al., 1987). Dinter and Schmitt (2001), after two years of GPS monitoring in Romania, found no significant deformation but recommended network expansion and repeated measurements at two-year intervals to better capture crustal dynamics. Van der Hoeven et al. (2005) later published results from annual GPS campaigns conducted between 1997 and 2004. However, velocity solutions derived from temporary GPS deployments were subject to influences such as equipment changes, monument removals, and antenna setup inconsistencies, as well as local effects like sediment compaction and site instability. Compared to the high precision of modern continuous GPS (cGPS) solutions, the historical campaign data exhibit 3 to 4 times higher uncertainty (van der Hoeven et al., 2005). These limitations highlight the need for continuous GPS measurements to better resolve crustal and mantle dynamics in geologically active regions.

2. Tectonic setting

The tectonic evolution of the Romanian region is essential for understanding present-day deformation and seismic activity. The Carpathian Mountains dominate the topography, but significant faulting and seismicity are pervasive in the South and Southeast Carpathians and the surrounding foreland (Petrescu et al., 2021), underlain by the MP, a thick lithospheric block with Precambrian-aged basement, shaped by multiple tectonic phases throughout the



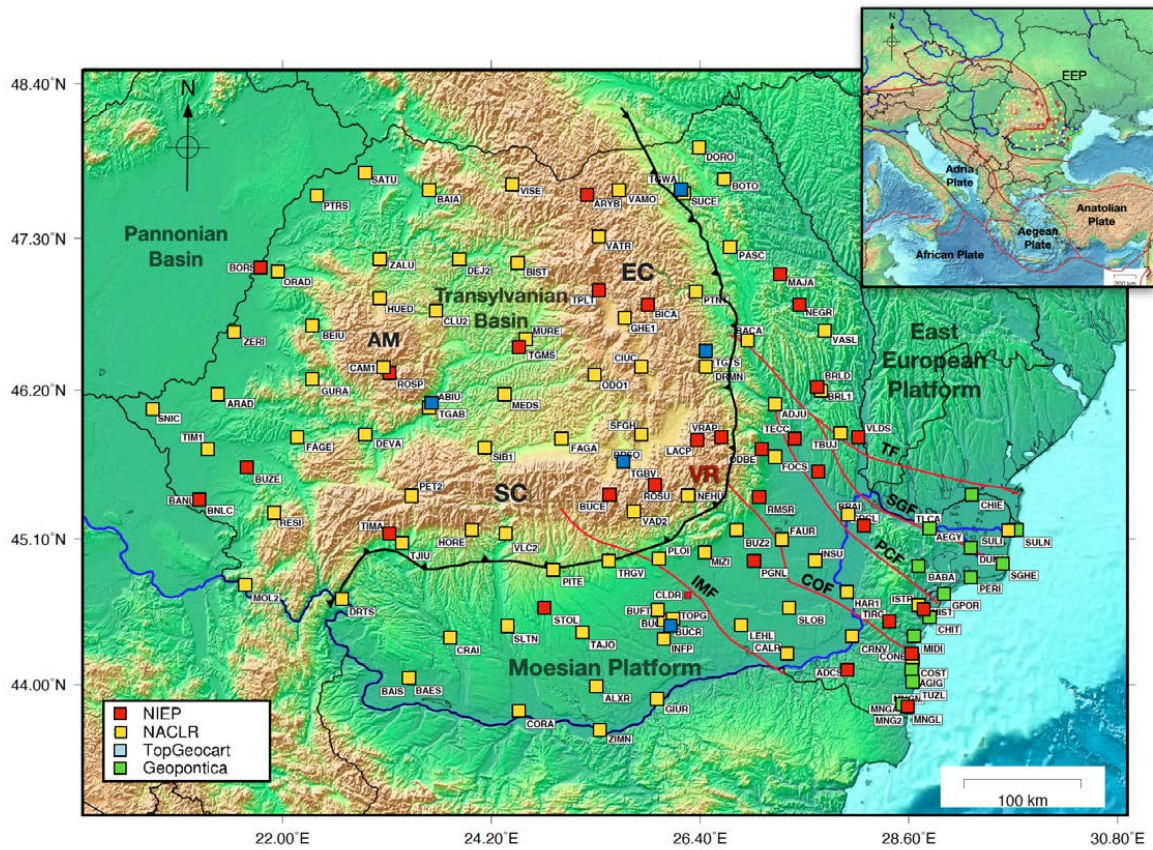
74 Paleozoic and Mesozoic times (Fig. 1). To the northeast, the MP transitions into the East European Platform
75 (EEP), a thick and geologically stable continental core that forms part of the Eurasian Plate. The boundary between
76 the two is marked by a series of crustal-scale faults and the North Dobrogea Orogen (NDO) (Hippolyte, 2002,
77 Fig. S1 in the Supplementary Material), a remnant of Hercynian Orogeny (Seghedi et al., 1999), located between
78 the Peceneaga-Camena Fault (PCF) and Sfântul Gheorghe Fault (SFG, Fig. 1). Part of this now partially eroded
79 orogen is buried beneath Neogene foredeep sediments from the younger Carpathian collision, while to the east, it
80 has undergone uplift.

81 Over the past 20 million years, the Adria Plate, a promontory of the African or Nubian plate, has continuously
82 pushed other oceanic plates and microplates north and east, leading to their collision with the stable Eurasian
83 terranes and driving the Alpine-Carpathian orogeny (Balla, 1986; Barrier et al. 2018), essentially shaping the
84 present-day European continent (Schmidt et al., 2020). In Romania, these microplates have been obliquely thrust
85 over the MP, forming the South Carpathians, and collided with the passive margin of the East European Platform,
86 creating a series of thrust faults and thin-skinned sedimentary nappes that make up the East Carpathians
87 (Sandulescu, 1984; Mațenco and Bertotti, 2000).

88 Beneath the Southeast Carpathians, where multiple tectonic units interact, the notorious Vrancea slab, a
89 lithospheric block that is plunging almost vertically into the mantle, stretching and generating frequent high-
90 magnitude destructive earthquakes in Romania, both at intermediate depths and in the overlying crust (Radulian
91 et al., 2019; Petrescu et al., 2021; Enescu et al., 2023). Observing the crustal motions above this sinking slab
92 provides a unique opportunity to gain fundamental insights into crustal deformation in a triple-junction tectonic
93 setting (Besutiu et al., 2019). Major collisional related shortening deformation in the Carpathians is thought to
94 have ended around 8–11 Ma, based on the cessation of late Miocene thrusting (Mațenco et al., 2007 and references
95 therein), while fission-track analysis suggests the onset of exhumation (or uplift) at 4 Ma in the SE Carpathians
96 and 12 Ma in the East and South Carpathians (Sanders et al., 1999; Cloetingh et al., 2006). Present-day GPS
97 measurements provide key insights into how these long-term geological processes continue to shape ongoing
98 crustal motion and deformation, particularly in the Vrancea Zone (Fig. 1), where active subduction and slab-
99 related dynamics are still influencing surface motion. The crustal deformations observed today are also influenced
100 by the relative motion of surrounding crustal blocks, complicating the understanding of the region's complex and
101 dynamic geological behavior.



102



103 **Figure 1: Map of Romania showing the distribution of cGPS stations used in this study (coloured squares), tectonic**
104 **regions, and major faults and tectonic boundaries (thick black lines). Abbreviations are: IMF- Intra-Moesian Fault,**
105 **COF- Căpârlău Ovidiu Fault, PCF- Peceneaga Cămin Fault, TF- Trotus Fault, SFG- Sfântu Gheorghe Fault, SC-**
106 **South Carpathians, EC- East Carpathians, VR - Vrancea, NIEP- National Institute for Earth Physics, NACLRL-**
107 **National Agency for Cadastre and Land Registration, GeoPonica- National Research-Development Institute for**
108 **Marine Geology and Geoecology GNSS network, TopGeocart private company GNSS network. The inset shows the**
109 **regional tectonic setting.**

110 3. Continuous GPS (cGPS) Networks in Romania

111 We analyze data from cGPS stations across Romania and surrounding regions, which are part of several
112 (Fig. 1). The primary network, supported by the National Institute for Earth Physics (NIEP), was first developed
113 in 2001. Initially, the network consisted of seven stations, equipped with Leica CRS1000 receivers and LEIAT504
114 choke-ring antenna protected by a dome. These stations were placed in remote areas and were designed to operate
115 with minimal maintenance, relying on power converters and batteries. Over time, the network has grown, and
116 today it includes 33 stations, with 5 of the original stations still in use. These newer stations are equipped with
117 Leica GRX1200, LEIAR GR30, and GR50 receivers, and are spread across Romania. Most of the antennas are
118 Leica (LEIAT504, LEIAR10, LEIAR20) and are placed on concrete pillars, only one is mounted on a polar mast



119 (MNG2). The stations transmit real-time data via the internet, and NIEP is responsible for the equipment,
120 installation, ongoing maintenance, and data analysis.

121 We also used GPS data from the GeoPontica network, developed by the National Research and Development
122 Institute for Marine Geology and Geoecology (GeoEcoMar), the National Center for Monitoring and Alarm to
123 Natural Marine Hazards – Euxinus, covering the period from 2013 to the present. This network includes 13
124 stations, the antennas are mounted on a deep-drilled braced monument. In addition, we included data from the
125 ROMPOS network, managed by the National Agency for Cadastral and Land Registration, which consists of 86
126 reference stations across Romania (Fig. 1). We were also granted access to data from the private TopGeocart
127 (TGRef) network, which includes 8 stations. Most of these GPS antennas are mounted on building rooftops or
128 integrated into the structures housing the receivers.

129 **4. GPS data processing**

130 For the data processing, we use the GipsyX software (Bertiger et al., 2020), developed at NASA's Jet Propulsion
131 Laboratory (JPL), Pasadena, USA. It features Precise Point Positioning (PPP), which enables (daily) geodetic
132 position determination of a single GPS station. Accuracy can vary depending on the quality of the GPS receiver,
133 the antenna, and local conditions (e.g. multipath). Weekly updated data files, provided by JPL, contain precise
134 GPS satellite orbits, Earth Rotation Parameters (ERP), satellite clock corrections, spacecraft altitude information,
135 and so-called wide lane phase biases to enable signal ambiguity resolution. In addition, we apply ocean loading
136 corrections for each station, obtained from Onsala Space Observatory, Chalmers University of Technology (Bos
137 and Scherneck). To model the wet tropospheric signal delays, we use data from VMF (Vienna Mapping Functions)
138 (re3data.org/VMF Data Server).

139 All available RINEX data files are stored in a database, organized by network, year, and Julian day. All cGPS
140 data used in this study are in the Receiver Independent Exchange (RINEX) version 2 and 3 format. To
141 homogenize the processing, we only use GPS data, sampled at a period of 30s. The processing with GipsyX
142 resulted in a similar database with daily solutions for each station (Fig. 2) in the ITRF14 reference frame
143 (Altamimi et al., 2016).

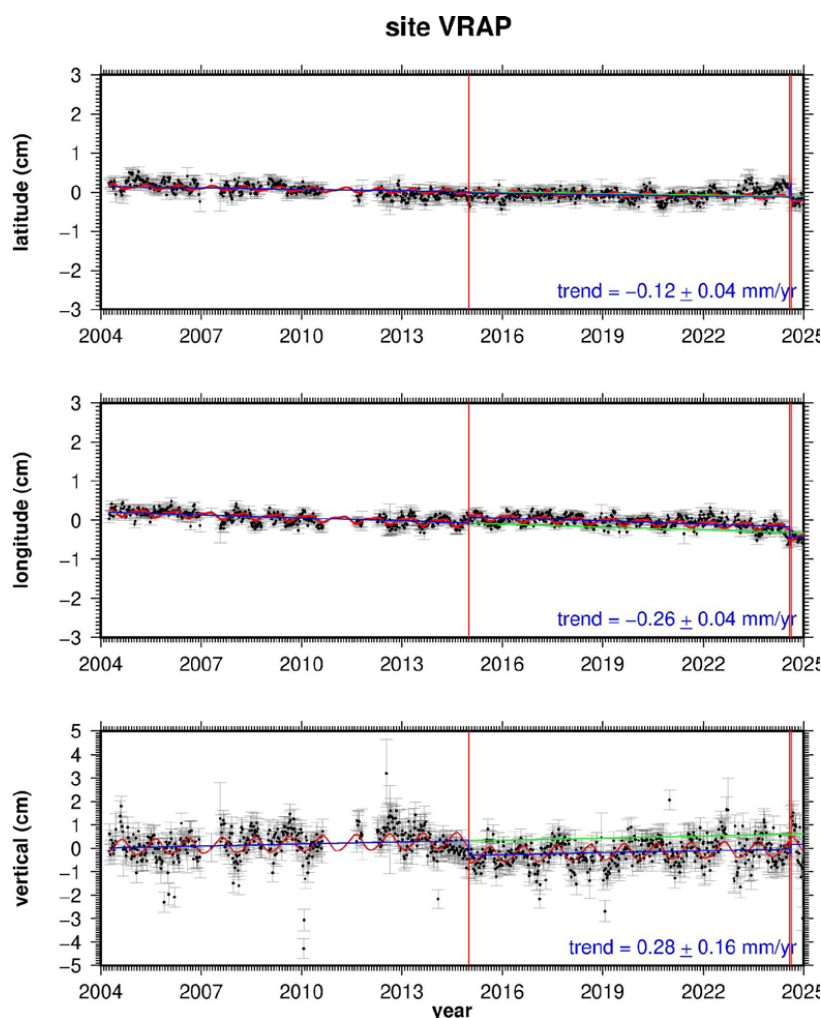


Figure 2: Time series of the VRAP station. The red curve represents the estimated yearly and half-yearly functions, the blue line indicates the estimated linear trend, and the green curve corresponds to the predicted values following the first jump. The vertical red lines represent position jumps.

To reduce the noise level, we combine the daily GPS positioning solutions into weekly solutions. Using our software, we convert these solutions to the Eurasian tectonic reference plate using the most recently published rotation pole solution of that plate. This results in a time series of latitude, longitude, and height components. From these time series, we calculate a linear trend (velocity) and yearly and half-yearly seasonal signals (Fig. 2).

To account for antenna changes that were not documented in the metadata, we also estimate position jumps at the times where we notice these changes (Fig. 2).

4.1 Horizontal data selection and quality control

Analysis of the 4 permanent Romanian networks resulted in 130 time series solutions for sites (still) operational after January 01, 2024. The length of the time series varies from 0.6 to 22.4 years. Then we apply a model to these



time series consisting of a linear term (the velocity), yearly and half yearly terms, and position jumps for undocumented antenna changes. Next, we apply a general editing criterion to only select solutions with an accuracy (sigma) of 0.2 mm/yr. This automatically eliminates the shorter lived time series, reducing the number of accepted solutions to 99, with the shortest series spanning 4.0 years. This means that all accepted solutions satisfy the criterion established by Blewitt et al. (2001), who claim that the series should be longer than 2.23 years for a reliable estimate of the seasonal terms, which is vital for the reliability of the velocity estimate.

The results for the 99 accepted sites are summarized in Table S1. Examples of a well-behaved site, BICA and ROSE, and problematic sites such as BRAI and STOL are given in Supplementary Material (Fig. S2 and S3). The latitude component of STOL also demonstrates that there can be significant seasonal variations, which can occur for any site and any component for unknown reasons. Part of the selection was a manual process, based on examining the time series plots for each site.

Finally, to ensure the best possible quality of the data, we selected results with uncertainties (sigmas) less than 0.2 mm/yr and velocity vectors smaller than 2 mm/yr. We consider that these criteria guarantee a reliable selection of credible solutions. A small number of these sites still exhibit anomalous velocities, likely caused by local effects such as landslides, station instability, local geological conditions, subsurface compaction, undocumented antenna changes, and multipath interference. The main reason is that most GPS antennas are mounted on buildings. Therefore, we added another editing step, described in the following paragraph.

4.2 Estimating a gridded, smoother horizontal velocity field

To derive a smoothed, coherent representation of the computed time series solutions, we use a spatial gridding approach: we set up an 8x8 grid of latitude and longitude nodes with each node linked to a square search box. The size of these boxes is based on the distance between neighbouring nodes, making sure the north-south and east-west dimensions are equal in kilometers. Inside each search box, we calculate the median of the absolute velocity vectors of the sites inside the box. In the next step, we eliminate outliers with a velocity larger than 2 times the median. In the final step, we calculate the average of the EW and NS velocity components of the remaining solutions. In this process, 22 of the 99 solutions are excluded as outliers. The final result is a gridded dataset showing velocities for each node, with some nodes left blank where no stations are available in the search area (Fig. 3).

When we include the literature (Pina-Valdes et al., 2022; Serpelloni et al., 2022), solutions for the countries neighbouring Romania, the number of solutions increases to 160. After applying the aforementioned editing step, this number decreases to 133. These solutions are based on a collection of shorter time series from before 2021. Nevertheless, they provide valuable additional information.

4.3 Vertical data selection

For the vertical component, we apply a different approach. This component is hardly affected by horizontal station instabilities, but mostly by undocumented antenna changes. We tackle this problem by estimating vertical position jumps at the dates we see them appearing in the time series. Furthermore, we only select solutions with an absolute velocity of < 2 mm/yr and an accuracy of < 1.0 mm/yr, which we consider to be credible solutions. Some sites



193 show larger subsidence, but these are mostly located in coastal areas, on slow landslides, and compacting
194 sedimentary areas. As a result, from the 130 available solutions of the four Romanian permanent networks, 106
195 solutions were accepted (Fig. 4).

196 When we include the literature solutions, the pattern does not change much. It mostly adds subsidence sites in the
197 area west and south-west of Romania (Table S2). The total number of accepted vertical sites increased to 156.

198 **4.4 Strain rate estimation**

199 To better understand deformation and seismic hazard in this complex tectonic region, we further estimate strain
200 rate from the interpolated horizontal vector field of GPS velocities (Fig. 3). We use the open-source software
201 STRAINTOOL, which employs the VISR (Velocity Interpolation for Strain Rate) algorithm developed by Shen
202 et al. (2015). This algorithm interpolates geodetic velocity data to derive horizontal strain rates across the region,
203 using a weighted least squares approach on a regular grid. At each site, the horizontal velocity field is
204 approximated by a bilinear function and a Gaussian function based on the distance between the interpolation site
205 is used for distance-weighting. This algorithm allows us to obtain the spatial variation of strain rate, including the
206 maximum shear strain rate (which indicates how much the crust is laterally distorted), and the dilatational strain
207 rate (which reflects areas of extension or compression). These parameters are crucial for understanding the
208 tectonic regime, whether a region is being compressed, extended, or sheared, and how this deformation relates to
209 observed earthquake focal mechanisms.

210 **5. Results**

211 **5.1 The horizontal velocity field**

212 Many horizontal velocity measurements indicate a predominantly southward movement in the MP, with variations
213 spanning approximately ± 20 degrees toward the southeast and southwest (Fig. 3). The IMF appears to mark a
214 slight orientation change from S-SE to S-SW oriented motion vectors. This shift is also reflected in the South
215 Carpathians, which are obliquely thrust over the MP, defined by strong and sometimes sharp lateral variation in
216 rheology across the major faults like IMF or COF, which imposed the formation of tear-faults and oblique ramps
217 into the Carpathian Orogen (Fig. 3). Hence, the magnitude and direction of motion vary significantly across the
218 IMF and COF or other major faults in the MP and foreland units in general, like PCF and TF, that are defining
219 crustal blocks with different rheologies, thermal history, and response under the orogenic loading. In contrast,
220 vectors in the East European Platform (EEP) appear to show a slight northwestward motion relative to the Eurasian
221 plate. This shift occurs across the PCF and TF, which define the boundaries of the North-Dobrogea Orogen (Fig.
222 3 and S1), a transitional zone between the EEP margin and the MP. As a result, the EEP undergoes a subtle yet
223 persistent movement relative to Eurasia, diverging from the southward-moving MP through a series of crustal-
224 scale faults that accommodate lateral displacement.

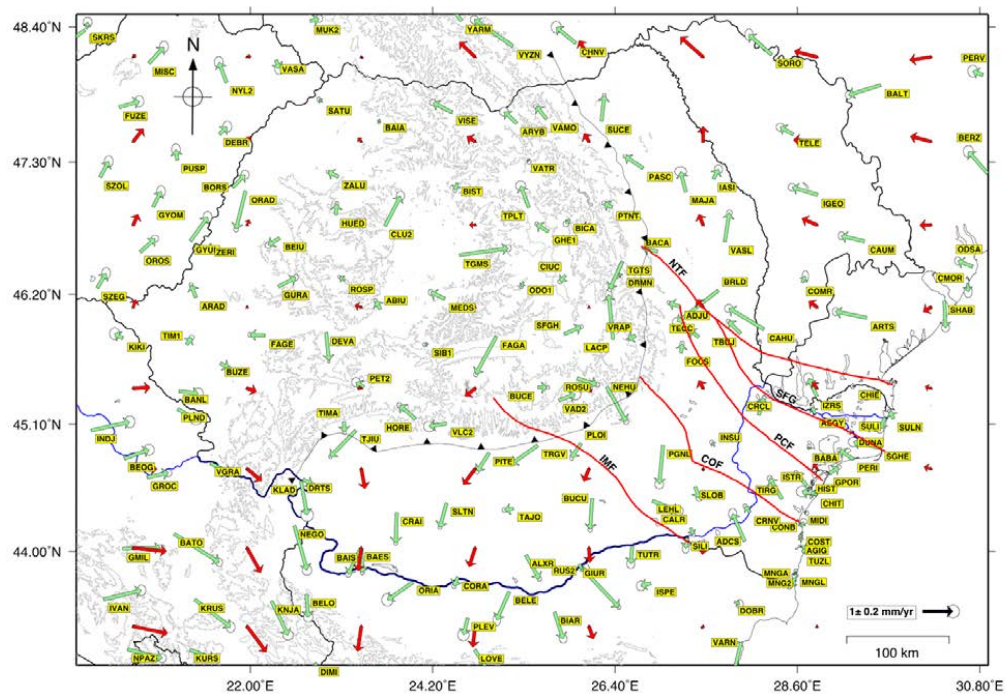


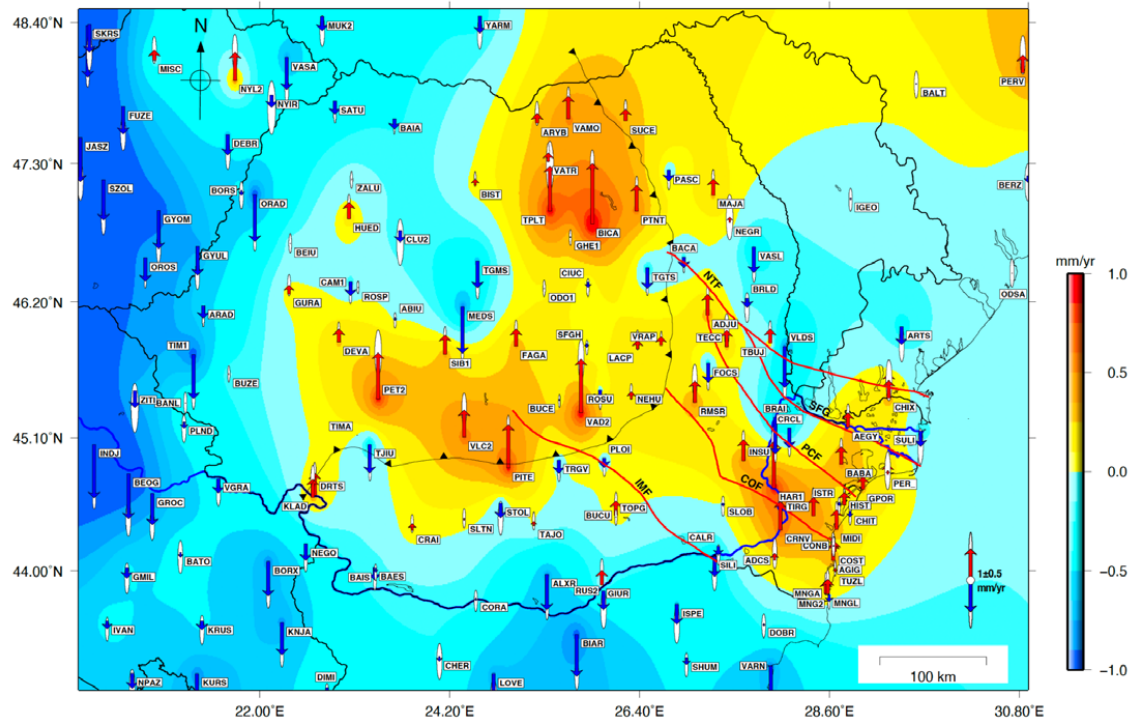
Figure 3: GPS-estimated horizontal velocity vectors with respect to the Eurasia Plate derived from the ITRF-2014 mapped solution. The error ellipses are 95% confidence level. Red arrows represent the interpolated vector field on a regular grid.

The Transylvanian Basin (TB) and the East Carpathians, on the other hand, show minimal horizontal motion. GPS stations in these areas indicate limited deformation, with inconsistent directional patterns and low overall coherence in movement. Small horizontal motions are observed in the Pannonian Basin (PB) with an NNE direction, which gets reoriented close to the Apuseni Mountains in different directions (see Figs 1 and 3).

Overall, the foreland region, particularly the MP, seems to be drifting southward, while the other areas remain relatively stable, indicating that the foreland is more dynamically active in comparison to the surrounding regions.



246 **5.2 The vertical velocity field**



247 **Figure 4: GPS-estimated vertical velocity vectors with respect to the Eurasia plate derived from the ITRF-2014 mapped**
248 **solution. The error ellipses are 95% confidence level. The major faults and tectonic boundaries are depicted by thick**
249 **red and black lines (abbreviations as in Fig. 1). A red vector indicates an upward motion, while a blue vector indicates**
250 **a downward motion.**

251 The Carpathians predominantly experience uplift, with the strongest upward velocity vectors concentrated in
252 localized areas of the East Carpathians (BICA, TPLT, see Fig. 4). Vertical motion stabilizes southward before
253 uplift resumes in the East Carpathians Bend Zone and the South Carpathians. While some scattered stations
254 (ROSU, TGTS) indicate subsidence, the overall trend suggests uplift rates ranging between 0.5 and 2 mm/yr. The
255 subsiding stations are located in the East Carpathians Bend Zone and Quaternary depressions and in the
256 Transylvanian Basin situated in the core of the Romanian Carpathians (Fig. 4).

257 The foreland has a more complex pattern, the Northern part of the EEP shows a slightly uplifting trend, in contrast
258 with its southern zone that is subsiding, a trend continues further South over the SFG and PCF (Fig. 4).

259 The MP situated in a foreland position relative to the Carpathians exhibits a complex interplay of uplift and
260 subsidence (Fig. 4). The crust appears to be subsiding in the south, gradually transitioning to an uplift trend closer
261 to the Carpathians and the COF. Northeast of the COF, several stations indicate uplift near the foredeep basin,
262 while the boundary with the EEP and southeastern Carpathians exhibits alternating zones of subsidence and uplift.
263 This transition creates a distinct pattern, with subsidence along the PCF and uplift near the TF. Toward the Black
264 Sea, vertical motion vectors suggest that the MP is undergoing consistent uplift in the coastal region (known as



265 Dobrogea). The Dobrogea region, including MP and NDO (see Fig. 1 and Fig. S1 in the Supplementary Material),
266 is experiencing uplift, defining a N-S trend different from the rest of the foreland system.

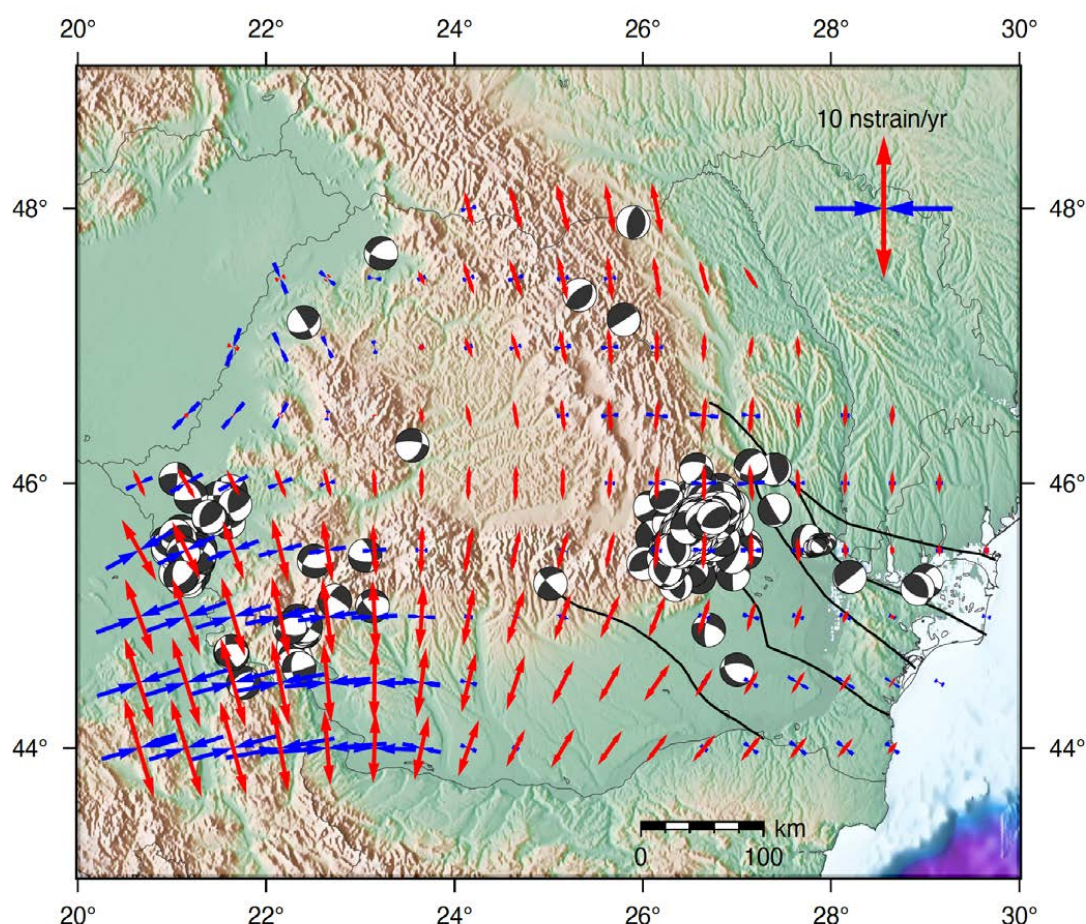
267 In the Transylvanian and Pannonian basins, estimated crustal motions suggest subsidence relative to stable
268 Eurasia. However, the Apuseni Mountains, a prominent highland dividing the two subsiding basins, exhibit a
269 cluster of stable and slightly uplifted motion vectors (Fig. 4).

270 **5.3 GPS-estimated strain rates**

271 Figure 5 shows the estimated strain rate variation across Romania, from the regularized horizontal velocity vector
272 field, while Fig. 6 a and b show the distribution of maximum shear strain rate and dilatation. The dilatation rate
273 quantifies the extent to which the Earth's crust is either expanding or contracting. It is derived by combining the
274 principal strain rates, with positive values indicating extension and negative values indicating contraction. High
275 positive dilatation values are indicative of regions experiencing extension, while negative values suggest
276 compression, as seen in processes like thrust faulting. On the other hand, the maximum shear strain rate measures
277 the degree of shear deformation within the crust, without affecting its overall volume. This is determined by
278 calculating the difference between the principal strain rates. Elevated shear strain rates are associated with regions
279 undergoing significant shear deformation, such as strike-slip fault zones, while lower values typically occur in
280 areas experiencing predominantly extensional or compressional deformation.



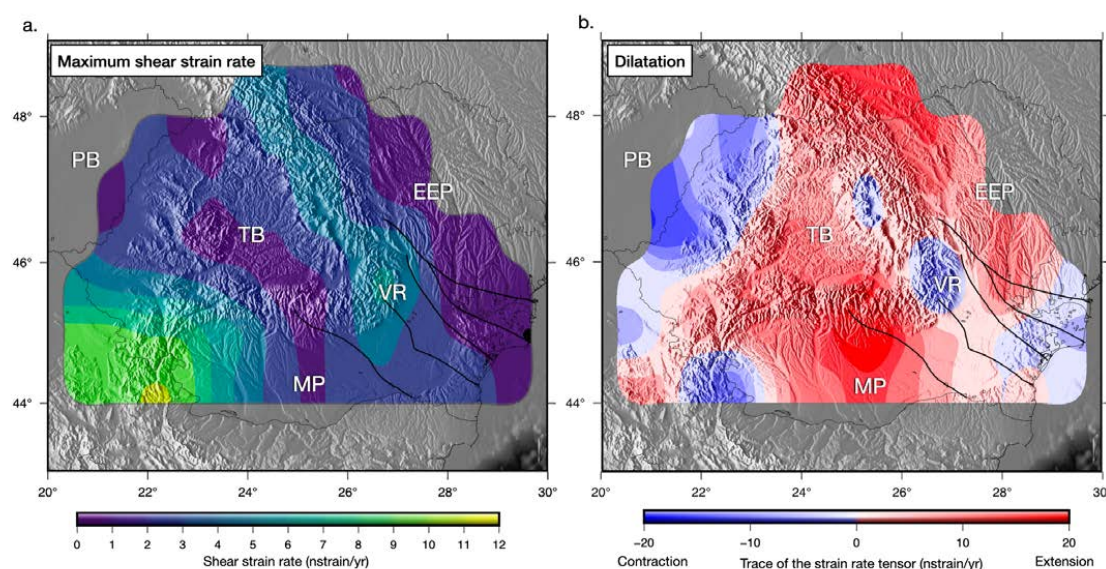
281



282 **Figure 5: Map showing the principal axes of strain rates determined from the smooth GPS horizontal**
 283 **velocity vector field from this study and mechanisms of earthquakes with $M_w > 3.5$ from the REFMC**
 284 **catalogue (Radulian et al., 2019). Major faults are depicted by thick black lines (see Figure 1).**

285 The distribution of strain rates is quite complex (Fig. 5), which is expected given the region's complicated tectonic
 286 framework, with multiple blocks of diverse strengths converging to form a sinuous orogenic track. The highest
 287 strain rates were estimated in the southwest, at the border between Romania and Serbia. This region also
 288 experiences the highest shear strain rate (Fig. 6a).

289 Dilatation patterns estimated from the strain tensor show a transition from compression in the PB to extension in
 290 the intra-orogenic TB. The South Carpathians and the surrounding foreland regions, including the MP and the
 291 EEP, are predominantly characterized by extension (Fig. 6b). However, localized areas of compression are
 292 observed in the Eastern and South-East Carpathians, particularly in the Vrancea Zone.



293

294 **Figure 6: Maps showing (a) maximum shear strain rate and (b) dilatational strain rate (both in**
 295 **nanostrain/year), derived from the average GPS velocity field in Romania. The maximum shear strain rate**
 296 **illustrates the intensity and direction of lateral crustal deformation, while the dilatational strain rate is the**
 297 **trace of the strain rate tensor (volumetric rate of change) and indicates regions of extension (red-positive)**
 298 **and compression (blue-negative). Major faults are shown as thick black lines (see Figure 1). Abbreviations**
 299 **are: PB - Pannonian Basin, TB - Transylvanian Basin, VR - Vrancea, MP - Moesian Platform, EEP -**
 300 **Eastern European Platform.**

301 6. Discussion

302 6.1 Regional tectonic context

303 To put our results in a broader context, we plot them in the context of previous GPS-derived velocity vectors
 304 (Serpeloni et al., 2022; Pina Valdes et al., 2022) in Fig. 7. While there is some overlap with the Romanian
 305 networks, the differences between datasets are minor. To reduce clutter in the figures and minimize the impact of
 306 large tectonic motions in the south, we excluded stations with an absolute horizontal velocity exceeding 7 mm/yr,
 307 as shown in Fig. 7a and 7b, with the UU-07 seismic tomography model of Amaru et al. (2007), updated based on
 308 Wortel and Spakman (2000), at 200 km depth, serving as background.

309

310

311

312

313

314

315

316

317

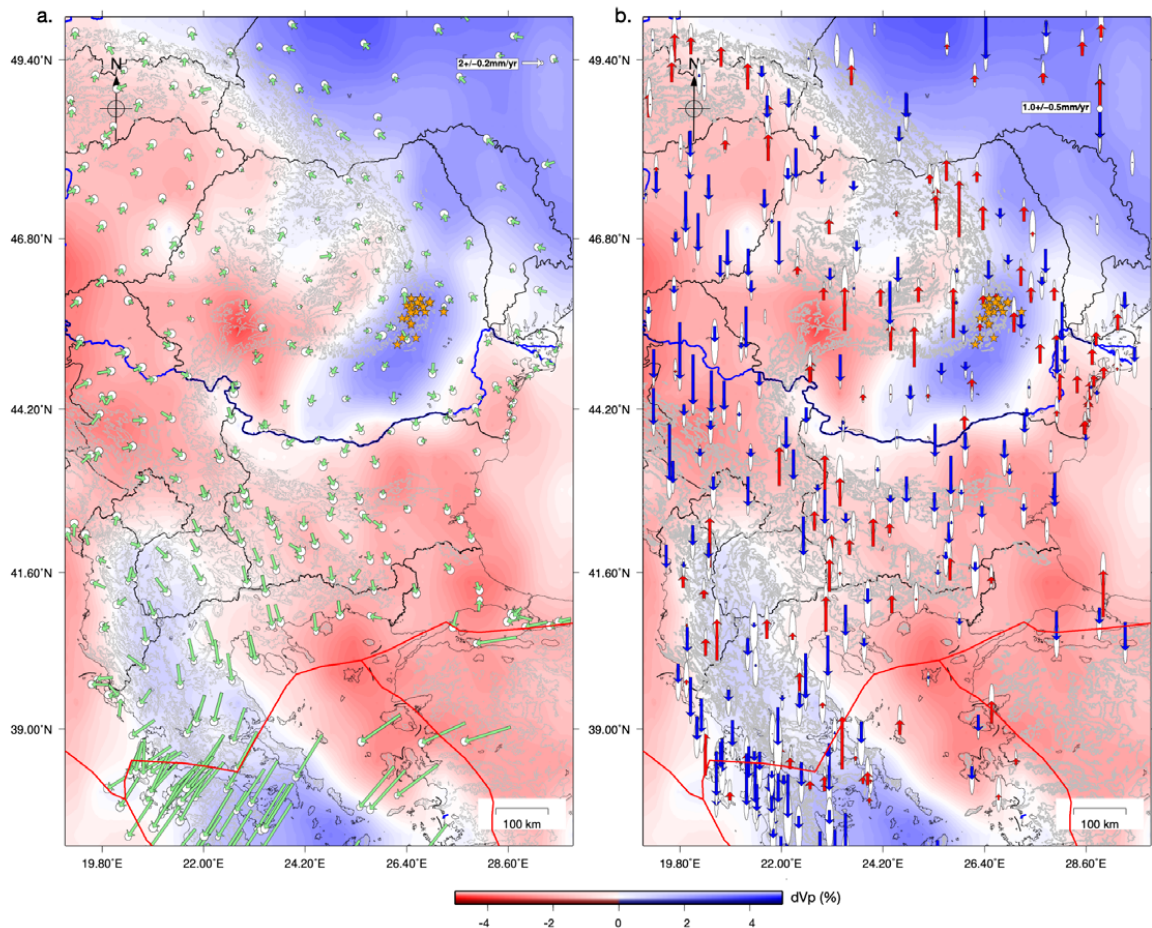


Figure 7: Regional horizontal (a) and vertical crustal motions (b) from this study, Serpeloni et al. (2022), and Pina
Valdes et al. (2022). The horizontal vector field was scaled for visibility. The background colours show Vp seismic
velocity anomalies at 200 km depth from the UU-P07 seismic model of Amaru et al. (2007). Red lines mark the active
plate boundaries between Eurasia, Anatolia, and Aegean plates in the south. Orange stars mark earthquakes Mw>6
from the Vrancea Zone (Radulian et al., 2019).

In the regional plate tectonic context, the observed velocity field highlights the complex interactions between major tectonic plates and blocks that converged in this complex region. Seismic tomography shows the high velocity thick cratonic lithosphere to the north-east, which is supposed to be tectonically stable, the Vrancea slab as an elongated high velocity block sinking beneath the Carpathians, and the Adria and the Hellenic slabs subducting beneath the Balkan peninsula (Fig. 7). To the south, crustal motion velocities increase significantly (Fig. 7), reflecting the rapid motion of the Hellenic subduction system as the African Plate subducts beneath the Eurasian Plate, driving southeastward deformation in Greece. Eastward, the Anatolian Plate is moving westward due to tectonic escape caused by the northward collision of the Arabian Plate with Eurasia. This westward motion is a dominant feature of the eastern Mediterranean and plays a key role in accommodating the overall regional deformation.



To the west, the Pannonian Basin, a hyper-thinned lithosphere back-arc basin, shows relatively low horizontal deformation rates, suggesting it is currently tectonically stable. However, the influence of the Adriatic plate, a promontory of the African Plate, is significant. The Adria plate, subducting eastwards (Fig. 7), exerts a northeastward push on the Carpathian-Pannonian system, contributing to compressional forces and tectonic inversion along the basin (Bada et al, 2007). These larger-scale processes interact with the local tectonic architecture, such as the Vrancea slab and associated seismicity (orange stars in Fig. 7), resulting in a complex and heterogeneous deformation regime that bridges the stable cratonic lithosphere and the active subduction-driven tectonics to the south and south-west.

6.2 Correlation with fault systems and seismicity

Most seismically active crustal-scale faults and geological boundaries in Romania are located in the South and South-East Carpathians, as well as the foreland domains, which are crossed by several major faults (Fig. 1). While the Vrancea slab is well known for generating subcrustal earthquakes with a dominant reverse faulting mechanism in an overall compressive regime, the crust above exhibits much more diverse deformation (Fig. 5) and stress patterns (Fig. 8), likely driven by a combination of surface plate kinematics and Vrancea slab dynamics.

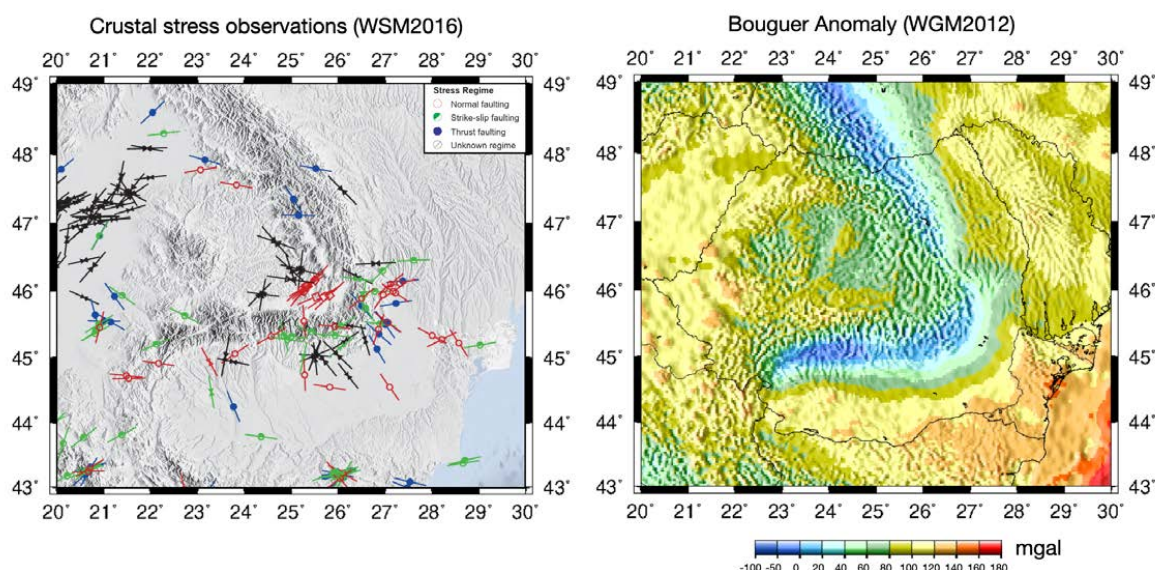


Figure 8: Left: Crustal stress observations compiled from focal mechanisms, borehole breakouts, and other geological indicators, from the World Stress Map (Heidbach et al., 2016). Colours indicate the most likely stress regime. Right: Bouguer gravity anomalies from the World Gravity Map (WGM2012) maintained by the Bureau Gravimétrique International (Bonvalot et al., 2012).

Stress inversion of earthquake clusters in the crust (Petrescu et al., 2021) and geological indicators of stress from the World Stress Map (WSM2016, Heidbach et al., 2007) reveal a complex pattern of stress in the region (Fig. 8). A localized cluster of thrust faulting stress regime indicators in the SE Carpathians broadly aligns with the negative dilatation rate derived from GPS vectors, suggesting localized compression at the bend zone (Fig. 6). This compressive region transitions into a mix of strike-slip and dominantly normal-faulting regimes (Fig. 8), aligning with our estimated dilatation rates that suggest an extensional regime throughout the foreland and the Carpathians



(Fig. 6). This extension is supported by numerous thrust-fault earthquake swarms occurring near the SFG (Craiu et al., 2017). The South Carpathians have also recently experienced an intense seismic swarm of thrust-faulting earthquakes in the South Carpathians (Borleanu et al., 2024). The compressive strain patch observed in the Eastern Carpathians (negative dilatation rate in Fig. 6b) coincides with a cluster of thrust faulting stress regime indicators (Fig. 8), reinforcing the reliability of the strain inversion derived from our estimated GPS velocities.

In the Moesian Platform, vertical movements are not uniform, but are accommodated differentially across crustal-scale fault systems. This variability likely arises from the differing rheological properties of crustal blocks that make up the MP (Mařenco et al., 2003; Petrescu et al., 2019) and the influence of pre-existing lithospheric heterogeneities (e.g., Bertotti et al., 2003; Tărăpoancă et al., 2004). As a result, many fault mechanisms in the MP exhibit both oblique and strike-slip components, producing seemingly chaotic fault patterns (Fig. 5). Moment tensor solutions in these regions may show greater variability, particularly in areas of pronounced strain partitioning, such as near large-offset faults or shear zones.

6.3 Interactions between slab dynamics and surface uplift

Our results indicate a clear uplift trend in the foredeep basin area, supporting a typical post-collisional rebound and uplift behavior, as observed in many other orogenic systems. These observations contrast with previous models (van der Hoeven, 2005; Merten, 2011), which suggest that subsidence dominated the evolution of the region as a typical response to slab subduction and retreat (Tărăpoancă et al., 2004). This is a key departure from earlier interpretations, which mainly focused on uplift in the Dobrogea forebulge while assuming subsidence further towards the Carpathian Orogen. This is also in line with some historical long-term repeated leveling methods (e.g., Popescu and Lazarescu, 1987; Joo, 1987). While the continued uplift in Dobrogea is confirmed, the GPS data suggest that this uplift extends into the foredeep, highlighting the presence of vertical motions in the foredeep basin that are not solely driven by active subduction dynamics.

The discrepancy may reflect either a shift in the tectonic regime over time or methodological limitations in capturing ongoing geodynamic processes. The observed uplift may be associated with a partial decoupling between the subducting lower lithosphere and the overlying crust (Petrescu et al., 2021), allowing stress relaxation and isostatic rebound of the upper crust in the foreland. This scenario is consistent with the distribution of intermediate-depth seismicity and the focal mechanism patterns observed in Vrancea. In addition, Mitrofan et al. (2014) suggested a partial transmission of deformation from the slab to the crust, further supporting the idea of vertical stress transfer from the mantle to the surface.

While the continued uplift in Dobrogea is confirmed, the GPS data suggest that this uplift extends into the foredeep, highlighting the presence of vertical motions in the foredeep basin that are not solely driven by active subduction dynamics. Instead, the observed uplift in both regions may be linked to slab break-off, a late-stage process in the subduction and continental collision cycle (Andrews and Billen, 2009). As mentioned before, the Dobrogea uplifting area at the transition to the Black Sea Basin is parallel with the SE Carpathians, suggesting again the interplay between collisional processes affecting the Orogen and flexural response of the lower plate with the forebulge outward (from the orogen) migration with coeval uplift and erosion.



393 Seismic imaging suggests that the Vrancea slab has partially torn and rotated at ~150 km depth (Martin et al.,
394 2006), leaving a deeper slab segment (200–310 km) still weakly attached (Heidbach et al., 2007). If break-off
395 continues to be active, asthenospheric upwelling through the torn slab segment (Petrescu et al., 2023) may be
396 dynamically supporting present-day uplift in both the SE Carpathians and foredeep. Numerical simulations of
397 subduction-collision systems with spontaneous slab break-off (Duretz et al., 2011) predict post-break-off uplift
398 rates of 0.1–0.8 km/Myr (0.1–0.8 mm/yr), which closely match our observed uplift. Additionally, an increase in
399 slab dip may promote low-wavelength lithospheric folding following continental collision (e.g., Cloetingh et al.,
400 2003; Mañenco et al., 2007), contributing further to the uplift observed in both the SE Carpathians and the
401 foredeep.

402 Our results also reveal a significant uplift in the East Carpathians (Fig. 4), not just the SE Carpathians, raising the
403 question of whether past slab break-off there could still be influencing present-day vertical motions. Geodynamic
404 reconstructions suggest that the subducted passive margin of the East European Platform progressively broke off
405 from north to south along the East Carpathians (Sperner et al., 1996), culminating in the currently detached
406 Vrancea slab. While the initial isostatic response to slab break-off is expected to occur within a few million years
407 (Duretz et al., 2011) or up to 7 million years after convergence stops (Andrews and Billen, 2009), prolonged
408 effects such as mantle flow, residual buoyancy, and lower-crustal flow could be sustaining regional uplift. This
409 interpretation is further supported by Bouguer gravity anomalies (Fig. 8), which show relatively positive values
410 (0–40 mGal) over the mountain belt, suggesting the presence of denser material at depth or incomplete isostatic
411 compensation. The north-to-south younging of post-collisional volcanism (Seghedi et al., 2004) suggests that slab
412 detachment propagated southward over time, with the East Carpathians experiencing earlier break-off than the SE
413 Carpathians. If asthenospheric upwelling and lithospheric weakening were significant during that time, they could
414 have led to prolonged crustal adjustments that continue to manifest as uplift today.

415 In addition to the SE and East Carpathians, we also identify localized uplift in the South Carpathians. This region
416 marks the collision between the Dacia Block and the Moesian Platform, where oblique thrusting over the thick
417 Moesian lithosphere (Mañenco et al., 1997) may be inducing flexural or isostatic responses (Bertotti et al., 2003).
418 Bouguer gravity anomalies in this area transition from strongly negative values (~–100 mGal) near the foredeep
419 in the south to over +100 mGal at the contact with the Transylvanian Basin (Fig. 8), indicating a shift from thick,
420 low-density crust to denser material in the north. This pattern suggests differential isostatic compensation, where
421 northward crustal thinning leads to less mass deficit and reduced buoyancy, potentially causing flexural uplift.
422 This contrast could drive vertical displacements, as observed. Alternatively, deeper mantle processes, such as
423 residual slab dynamics or lithospheric-scale deformation associated with orogenic curvature, may also influence
424 the observed uplift.

425
426
427
428
429
430



431 **7. Conclusions**

432 This study integrates the most stable and longest GPS data records over a period of 20 years in the Carpathian
433 region in Romania. Our results mark a significant improvement in spatial coverage and resolution of vertical and
434 horizontal crustal motions in a tectonically complex region sitting at the transition between dynamically active
435 subduction systems and the stable East European Platform, with additional influences exerted by a descending
436 slab.

437 We observe significant horizontal southward motion in the Moesian Platform, minimal motion in the
438 Transylvanian Basin and East Carpathians, and a slight north-west motion of the Eastern European Platform, in a
439 Eurasian reference frame. The relative motions between these regions generate a complex strain rate pattern with
440 zones of extension, compression, and shear, which closely align with observed regional seismic activity.

441 Our extended and more reliable data also reveal uplift in the foredeep of the SE Carpathians, challenging a
442 previously-held view that this area is solely subsiding based on temporary GPS station data. This insight provides
443 a fresh perspective on the region's slab dynamics, which may be influenced by slab break-off and the fragmented
444 nature of the foreland, with its blocks of varying rheological strength. These differential vertical motions are
445 accommodated by seismically active faults on a crustal scale.

446 Overall, this study significantly advances our understanding of the tectonic processes that shape regions at the
447 intersection of active subduction/collision zones and stable continental platforms. It provides fundamental
448 constraints on the interplay between slab dynamics, surface plate kinematics, and the resulting crustal
449 deformation, an essential step toward improving seismic hazard assessment.

450

451 **Code availability**

452 The GipsyX software is licensed to the Department of Geophysics of the University of Bucharest (UNIBUC). We
453 were allowed to use this software in an ongoing collaboration with UNIBUC. Strain rate estimation codes are
454 freely available at <https://github.com/DSOlab/StrainTool> (accessed in January 2025). Most figures were made
455 using the open-source GMT software (Wessel et al., 2013).

456

457 **Data availability**

458 The data that support the findings of this study are available from the corresponding author upon reasonable
459 request.

460

461 **Author contributions**

462 **AM:** Conceptualization, Methodology, Data Curation, Formal analysis, Investigation, Writing - Original Draft,
463 Visualization **LP:** Formal analysis, Writing - Original Draft, Visualization **BA:** Software, Data Curation, Formal
464 analysis, Visualization, Writing - Review & Editing, Supervision **FB:** Writing - Review & Editing **EN:** Writing -
465 Review & Editing, Installation and Stations Maintenance **IM:** Writing - Review & Editing

466

467 **Competing interests**

468 The authors declare that they have no conflict of interest.



469 **Acknowledgments**

470 We gratefully acknowledge Prof. Dr. V. Mocanu, who, in 2001, initiated the establishment of the first seven
471 dedicated continuous GPS (cGPS) stations in Romania, together with our esteemed late colleague L. Munteanu
472 and a consortium of Dutch universities. Their early efforts laid the groundwork for long-term geodetic and
473 geophysical research in the region. We thank the National Research and Development Institute for Marine
474 Geology and Geo-Ecology, National Center for Monitoring and Alarm to Natural Marine Hazards – Euxinus, as
475 well as the National Agency for Cadaster and Land Registration, and the TopGeocart company for providing
476 access to their data.

477

478 **Financial support**

479 This research was carried out within the NUCLEU project, SOL4RISC Program which is supported by the
480 Ministry of Education and Research, project nr. PN23360201. This work was also supported by the European
481 Union (Next Generation EU instrument) through the National Recovery and Resilience Plan, "PNRR-III-C9-2022
482 – I5 Establishment and operationalization of Competence Centers" competition, "Competence Center for Climate
483 Change Digital Twin for Earth forecasts and societal redressment: DTEClimate" project, contract
484 no.760008/30.12.2022, code 7/16.11.2022.

485 **References**

- 486 Altamimi, Z., Rebischung, P., Métivier, L., Collilieux, X.: ITRF2014: a new release of the International
487 Terrestrial Reference Frame modeling nonlinear station motions, *J. Geophys. Res.-Sol. Ea.*, 121, 6109–6131,
488 <https://doi.org/10.1002/2016JB013098>, 2016.
- 489 Amaru, M. L.: Global travel time tomography with 3-D reference models, PhD thesis, Utrecht Univ., Utrecht,
490 Netherlands, 2007.
- 491 Andrews, E. R. and Billen, M. I.: Rheologic controls on the dynamics of slab detachment, *Tectonophysics*, 464,
492 60–69, <https://doi.org/10.1016/j.tecto.2007.09.004>, 2009.
- 493 Armeanu, I., Chircea, A., Ciobanu, I., Craiu, A., Craiu, G. M., Dinescu, R., Mihai, M., Predoiu, A., Tolea,
494 A., Varzaru, L. C., Borleanu, F., Neagoe, C., Radulian, M., Mihaela, P.: Database of the 2023 seismic sequence
495 recorded in Gorj area (Romania), Mendeley Data, V1, <https://doi.org/10.17632/ds4hwchkp7.1>, 2023.
- 496 Bada, G., Horváth, F., Dövényi, P., Szafián, P., Windhoffer, G. and Cloetingh, S.: Present-day stress field and
497 tectonic inversion in the Pannonian basin, *Global Planet. Change*, 58, 165–180,
498 <https://doi.org/10.1016/j.gloplacha.2007.01.007>, 2007.
- 499 Balla, Z.: Palaeotectonic reconstruction of the central Alpine-Mediterranean belt for the Neogene,
500 *Tectonophysics*, 127, 213–243, [https://doi.org/10.1016/0040-1951\(86\)90062-4](https://doi.org/10.1016/0040-1951(86)90062-4), 1986.
- 501 Bertiger, W., Bar-Sever, Y., Dorsey, A., Haines, B., Harvey, N., Hemberger, D., Heflin, M., Lu, W., Miller, M.,
502 Moore, A. W., Murphy, D., Ries, P., Romans, L., Sibois, A., Sibthorpe, A., Szilagyi, B., Vallisneri, M., and Willis,
503 P.: GipsyX/RTGx, a new tool set for space geodetic operations and research, *Advances in Space Research*, 66,
504 469–489, <https://doi.org/10.1016/j.asr.2020.04.015>, 2020.
- 505 Bertotti, G., Maţenco, L. and Cloetingh, S. A. P. L.: Vertical movements in and around the south-east Carpathian
506 foredeep: lithospheric memory and stress field control. *Terra Nova*, 15, 299–305, 2003.
- 507 Blewitt, G., Lavallée, D., Clarke, P., and Nurutdinov, K.: A new global mode of Earth deformation: Seasonal
508 cycle detected, *Science*, 294, 2.342–2.345, <https://doi.org/10.1126/science.106532001>, 2001.
- 509 Bonvalot, S., Balmino, G., Briais, A., M. Kuhn, Peyrefitte, A., Vales, Biancale, R., Gabalda, G., Moreaux, G.,
510 Reinquin, F., Sarrailh, M.: World Gravity Map. 1:50000000 map, Eds.: BGI-CGMW-CNES-IRD, Paris, 2012.



- 511 Bos. M., S., Scherneck, H., G., Chalmers University of Technology, Ocean tide loading provider,
512 <http://holt.oso.chalmers.se/loading/index.html>.
- 513 Borleanu F., Petrescu L., Fojtikova L., Munteanu I., Silvennoinen H., Placinta A.O., Oros E., Enescu B.: ML 5.7
514 Southern Carpathians earthquake sequence: Insights from seismic observations, ESC2024-S17/50-808,
515 https://www.erasmus.gr/UsersFiles/microsite1277/Documents/ESC2024_Abstract_Book.pdf, 2024.
- 516 Cloetingh, S.A.P.L., Burov, E., Matenco, L., Toussaint, G., Bertotti, G., Andriessen, P.A.M., Wortel, M.J.R. and
517 Spakman, W.: Thermo-mechanical controls on the mode of continental collision in the SE Carpathians (Romania),
518 *Earth Planet. Sc. Lett.*, 218, 57-76, 2004.
- 519 Cloetingh, S., Bada, G., Maţenco, L., Lankreijer, A., Horváth, F. and Dinu, C.: Modes of basin (de) formation,
520 lithospheric strength and vertical motions in the Pannonian-Carpathian system: inferences from thermo-
521 mechanical modelling, *Geo. Soc. Mem.*, 32, 207-221, DOI: 10.1144/GSL.MEM.2006.032.01.12, 2006.
- 522 Cornea, I., Dragoescu, I., Popescu, M. N., Visarion, M.: Monography of recent vertical crustal movements in the
523 S. R. of Romania (in Romanian), Preprint Central Inst. of Phys., 100, 1978.
- 524 Cornea, I., and Popescu, M. N.: The Vrancea Earthquake of March 4. 1977 and the Recent crustal vertical
525 movements in Romania. In Cornea & Radu (Editors): Seismological Research of March 4. 1977 Earthquake (in
526 Romanian), Preprint Central Inst. of Phys., 559 - 568, 1979.
- 527 Cornea, I., Dragoescu, I., Popescu, M. N., Visarion, M.: Map of recent vertical crustal movements of the territory
528 of S. R. of Romania (in Romanian), *St. Cerc. Geol., Geofiz., Geogr., Geofizica*, 17, 3-20, 1979.
- 529 Craiu, A., Craiu, M., Diaconescu, M. and Marmureanu, A.: 2013 Seismic swarm recorded in Galati area,
530 Romania: focal mechanism solutions, *Acta Geod. Geophys.*, 52, 53-67, 2017.
- 531 Csontos, L., and Vörös, A.: Mesozoic plate tectonic reconstruction of the Carpathian region, *Palaeogeography,*
532 *Palaeoclimatology, Palaeoecology*, 210, 1-56, <https://doi.org/10.1016/j.palaeo.2004.02.033>, 2004.
- 533 Dinter, G., Schmitt, G.: Three Dimensional Plate Kinematics in Romania, *Nat. Hazards*, 23, 389-406,
534 <https://doi.org/10.1023/A:1011116615142>, 2001.
- 535 Duretz, T., Gerya, T.V. and May, D.A.: Numerical modelling of spontaneous slab breakoff and subsequent
536 topographic response, *Tectonophysics*, 502, 244-256, <https://doi.org/10.1016/j.tecto.2010.05.024>, 2011.
- 537 Heidbach, O., Ledermann, P., Kurfeß, D., Peters, G., Buchmann, T., Matenco, L., Negut, M., Sperner, B., Müller,
538 B., Nuckelt, A., et al.: Attached or not attached: slab dynamics beneath Vrancea, Romania, In: International
539 symposium on strong Vrancea earthquakes and risk mitigation, 4-20, 2007.
- 540 Hippolyte, J.C.: Geodynamics of Dobrogea (Romania): new constraints on the evolution of the Tornquist-
541 Teisseyre Line, the Black Sea and the Carpathians, *Tectonophysics*, 357, 33-53, [https://doi.org/10.1016/S0040-1951\(02\)00361-X](https://doi.org/10.1016/S0040-1951(02)00361-X), 2002.
- 543 Ionescu, C., and Neagoe, C.: Romanian seismic network development, *Acta Geod. Geophys. Hu.*, 43, 145-152
544 DOI: 10.1556/AGeod.43.2008.2-3.4, 2008.
- 545 Ismail-Zadeh, A., Maţenco, L., Radulian, M., Cloetingh, S. and Panza, G.: Geodynamics and intermediate-depth
546 seismicity in Vrancea (the south-eastern Carpathians): current state-of-the art. *Tectonophysics*, 530, 50-79, DOI:
547 10.1016/j.tecto.2012.01.016, 2012.
- 548 Joó, I., Arabadžijski, D., Füry, M., Meščerski, I. N., Mihăila, M., Mladenovski, M. M., Németh, Z., Steinberg, J.,
549 Thury, J., Vanko, J., & Wyrzykowski, T.: New investigations or recent vertical movements in the Carpatho-
550 Balkan region, *J. Geodyn.*, 8, 99-113, [https://doi.org/10.1016/0264-3707\(87\)90028-7](https://doi.org/10.1016/0264-3707(87)90028-7), 1987.
- 551 Koulakov, I., Zaharia, B., Enescu, B., Radulian, M., Popa, M., Parolai, S. and Zschau, J.: Delamination or slab
552 detachment beneath Vrancea? New arguments from local earthquake tomography, *Geochem. Geophys. Geosys.*,
553 11, <https://doi.org/10.1029/2009GC002811>, 2010.
- 554 Krézsek, C., Lăpădat, A., Maţenco, L., Arnberger, K., Barbu, V., Olaru, R.: Strain partitioning at orogenic contacts
555 during rotation, strike-slip and oblique convergence: Paleogene-Early Miocene evolution of the contact between
556 the South Carpathians and Moesia, *Global Planet. Change*, 103, 63-81, <https://doi.org/10.1016/j.gloplacha.2012.11.009>, 2013.



- 558 Lorinczi, P., Houseman, G.: Lithospheric gravitational instability beneath the Southeast Carpathians,
559 Tectonophysics, 474, 322–336, <https://doi.org/10.1016/j.tecto.2008.05.024>, 2009.
- 560 Mațenco, L., Bertotti, G.: Tertiary tectonic evolution of the external East Carpathians (Romania), Tectonophysics,
561 316, 255–286, [https://doi.org/10.1016/S0040-1951\(99\)00261-9](https://doi.org/10.1016/S0040-1951(99)00261-9), 2000.
- 562 Mațenco, L., Bertotti, G., Leever, K., Cloetingh, S.A.P.L., Schmid, S.M., Tărăpoancă, M. and Dinu, C.: Large-
563 scale deformation in a locked collisional boundary: Interplay between subsidence and uplift, intraplate stress, and
564 inherited lithospheric structure in the late stage of the SE Carpathians evolution, Tectonics, 26,
565 <https://doi.org/10.1029/2006TC001951>, 2007.
- 566 Mrazec L., Voitești I.P.: Contributii la cunoasterea panzelor flisului carpatic (in Romanian), An. Inst. Geol. Rom.,
567 V, 495–521, 1914.
- 568 Müller, B., Heidbach, O., Negut, M., Sperner, B. and Buchmann, T.: Attached or not attached—evidence from
569 crustal stress observations for a weak coupling of the Vrancea slab in Romania, Tectonophysics, 482, 139–149,
570 <https://doi.org/10.1016/j.tecto.2009.08.022>, 2010.
- 571 Nemcok, M., Pospisil, L., Lexa, J. and Donelick, R.A.: Tertiary subduction and slab break-off model of the
572 Carpathian–Pannonian region, Tectonophysics, 295, 307–340, [https://doi.org/10.1016/S0040-1951\(98\)00092-4](https://doi.org/10.1016/S0040-1951(98)00092-4),
573 1998.
- 574 Petrescu, L., Borleanu, F., Radulian, M., Ismail-Zadeh, A. and Mațenco, L.: Tectonic regimes and stress patterns
575 in the Vrancea Seismic Zone: Insights into intermediate-depth earthquake nests in locked collisional settings,
576 Tectonophysics, 799, 228688, <https://doi.org/10.1016/j.tecto.2020.228688>, 2021.
- 577 Petrescu, L., Stuart, G., Tataru, D., and Grecu, B.: Crustal structure of the Carpathian Orogen in Romania from
578 receiver functions and ambient noise tomography: how craton collision, subduction and detachment affect the
579 crust. Geophys. J. Int., 218, 163–178, <https://doi.org/10.1093/gji/ggz140>, 2019.
- 580 Petrescu, L., Mihai, A. and Borleanu, F.: Slab tear and rotation imaged with core-refracted shear wave anisotropy.,
581 J. Geodyn., 157, 101985, <https://doi.org/10.1016/j.jog.2023.101985>, 2023.
- 582 Piña-Valdés, J., Socquet, A., Beauval, C., Doin, M.-P., D’Agostino, N., & Shen, Z.-K.: 3D GNSS velocity field
583 sheds light on the deformation mechanisms in Europe: Effects of the vertical crustal motion on the distribution of
584 seismicity, J. Geophys. Res.-Sol. Ea., 127, e2021JB023451, <https://doi.org/10.1029/2021JB023451>, 2022.
- 585 Popa, M., Chircea, A., Dinescu, R., Neagoe, C., Grecu, B. and Borleanu, F.: Romanian earthquake catalogue
586 (ROMPLUS). *Mendeley Data*, 2, 2022.
- 587 Popescu, M. N., & Drăgoescu, I.: Maps of recent vertical crustal movements in Romania: Similarities and
588 differences, J. Geodyn., 8, 123–136, [https://doi.org/10.1016/0264-3707\(87\)90030-5](https://doi.org/10.1016/0264-3707(87)90030-5), 1987.
- 589 Radulescu F.: Romanian seismology – historical, scientific and human landmarks Rev. Roum. Geophysique, 52–
590 53, 101–121, 2008–2009.
- 591 Radulian, M., Bălă, A., Ardeleanu, L., Toma-Dănilă, D., Petrescu, L. and Popescu, E.: Revised catalogue of
592 earthquake mechanisms for the events occurred in Romania until the end of twentieth century: REFMC, Acta
593 Geod. Geophys., 54, 3–18, <https://doi.org/10.1007/s40328-018-0243-y>, 2019.
- 594 Ren, Y., Stuart, G., Houseman, G., Dando, B., Ionescu, C., Hegedüs, E., Radovanović, S., Shen, Y., S. C. P. W.
595 Group, et al.: Upper mantle structures beneath the Carpathian–Pannonian region: Implications for the
596 geodynamics of continental collision, Earth Planet. Sc. Lett., 349, 139–152. <https://doi.org/10.1016/j.epsl.2012.06.037>, 2012.
- 598 re3data.org: VMF Data Server; editing status 2024-05-15; re3data.org - Registry of Research Data Repositories,
599 <https://doi.org/10.17616/R3RD2H>
- 600 Sanders, C., Andriessen, P., & Cloetingh, S.: Life cycle of the East Carpathian orogen: erosion history of a doubly
601 vergent critical wedge assessed by fission track thermochronology, J. Geophys. Res., 104, 29095–29112,
602 <https://doi.org/10.1029/1998JB900046>, 1999.
- 603 Schmid, S.M., Fügenschuh, B., Kounov, A., Mațenco, L., Nievergelt, P., Oberhänsli, R., Pleuger, J., Schefer, S.,
604 Schuster, R., Tomljenović, B. and Ustaszewski, K.: Tectonic units of the Alpine collision zone between Eastern
605 Alps and western Turkey, Gondwana Res., 78, 308–374, <https://doi.org/10.1016/j.gr.2019.07.005>, 2020.



- 606 Seghedi, A., Lang, B. and Heimann, A.: The deformational history of North Dobrogean Hercynian basement as
607 reflected in new ³⁹Ar/⁴⁰Ar determinations, *Romanian Journal of Tectonics and Regional Geology*, 77, 64-65,
608 <https://doi.org/10.3906/YER-1101-20>, 1999.
- 609 Seghedi, I., Downes, H., Vaselli, O., Szakács, A., Balogh, K. and Pécskay, Z.: Post-collisional Tertiary–
610 Quaternary mafic alkaline magmatism in the Carpathian–Pannonian region: a review, *Tectonophysics*, 393, 43-62,
611 <https://doi.org/10.1016/j.tecto.2004.07.051>, 2004.
- 612 Serpelloni, E., Cavaliere, A., Martelli, L., Pintori, F., Anderlini, L., Borghi, A., Randazzo, D., Bruni, S., Devoti,
613 R., Perfetti, P., & Cacciaguerra, S.: Surface Velocities and Strain-Rates in the Euro-Mediterranean Region From
614 Massive GPS Data Processing, *Front. Earth Sci.*, 10, 907897, <https://doi.org/10.3389/feart.2022.907897>, 2022.
- 615 Sperner, B.: Computer programs for the kinematic analysis of brittle deformation structures and the Tertiary
616 tectonic evolution of the Western Carpathians. Tübingen Geoscientific Works (TGA) Series A. Geology,
617 Paleontology, Stratigraphy 27 (NEBIS)001536648EBI01, 1996.
- 618 Sperner, B., Lorenz, F., Bonjer, K., Hettel, S., Müller, B. and Wenzel, F.: Slab break-off–abrupt cut or gradual
619 detachment? New insights from the Vrancea Region (SE Carpathians, Romania), *Terra Nova*, 13, 172-179,
620 <https://doi.org/10.1046/j.1365-3121.2001.00335.x>, 2001.
- 621 Tărăpoancă, M., Garcia-Castellanos, D., Bertotti, G., Matenco, L., Cloetingh, S., Dinu, C.: Role of the 3-D
622 distributions of load and lithospheric strength in orogenic arcs: polystage subsidence in the Carpathians foredeep,
623 *Earth Planet. Sc. Lett.*, 221, 163–180, [https://doi.org/10.1016/S0012-821X\(04\)00068-8](https://doi.org/10.1016/S0012-821X(04)00068-8), 2004.
- 624 Van der Hoeven, A., Mocanu, V., Spakman, W., Nutto, M., Nuckelt, A., Matenco, L., Munteanu, L., Marcu, C.,
625 & Ambrosius, B.: Observation of present-day tectonic motions in the Southeastern Carpathians: Results of the
626 ISES/CRC-461 GPS measurements, *Earth Planet. Sc. Lett.*, 239, 177-
627 184, <https://doi.org/10.1016/j.epsl.2005.09.018>, 2005.
- 628 Wenzel, F., Lorenz, F., Sperner, B., and Oncescu, M. C.: Seismotectonics of the Romanian Vrancea area, Vrancea
629 Earthquakes: Tectonics, Hazard and Risk Mitigation, 15–26, Kluwer Acad., 1999.
- 630 Wessel, P., W. H. Smith, R. Scharroo, J. Luis, and F. Wobbe: Generic mapping tools: improved version released,
631 *Eos, Transactions American Geophysical Union*, 94 (45), 409–410, 2013.
- 632 Wortel, M.J.R. and Spakman, W.: Subduction and slab detachment in the Mediterranean-Carpathian region,
633 *Science*, 290, 1910-1917, <https://doi.org/10.1126/science.290.5498.1910>, 2000.
- 634 Zandt, G., Gilbert, H., Owens, T.J., Ducea, M., Saleeby, J., and Jones, C.H.: Active foundering of a continental
635 arc root beneath the southern Sierra Nevada in California. *Nature*, 431, 41–46, <https://doi.org/10.1038/nature02847>,
636 2004.